Supporting Information

H/D isotope effects reveal factors controlling catalytic activity in Co-based oxides for water oxidation

Chiara Pasquini[1], Ivelina Zaharieva[1], Diego González-Flores[1], Petko Chernev[1], Mohammad Reza Mohammadi[1,2], Leonardo Guidoni[3], Rodney D. L. Smith[*1,4], Holger Dau[*1]

[1] Department of Physics, Freie Universität Berlin, Arnimallee 14, 14195 Berlin (Germany).
[2] Department of Physics, University of Sistan and Baluchestan, Zahedan, 98167-45845 (Iran).
[3] Dipartimento di Scienze Fisiche e Chimiche, Università degli studi dell'Aquila,Via Vetoio (Coppito), 67100 L'Aquila (Italy).
[4] Department of Chemistry, University of Waterloo, 200 University Ave. W, N2L 3G1 Waterloo, ON (Canada).

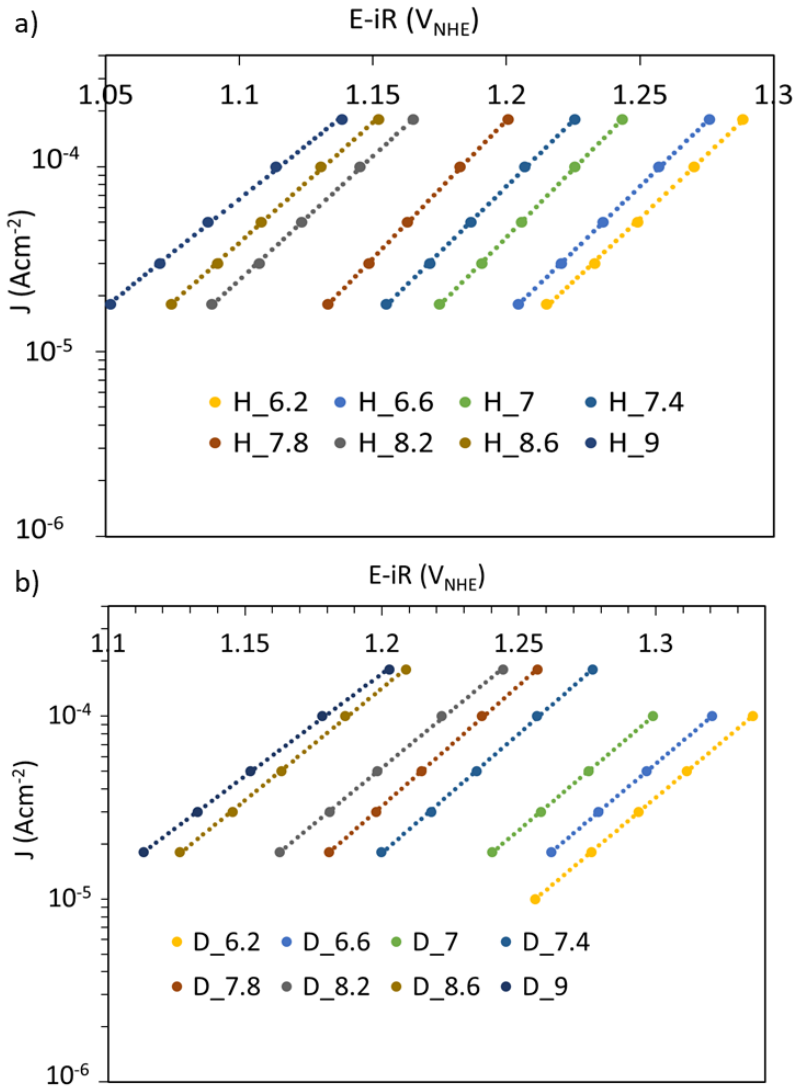

Figure S1. Tafel plot from steady state (values taken after 3 min) chronopotentiometry measurements of CoCat in the neutral pH regime (5<pL<9) in 0.1 M KPi made of (a) water and (b) deuterated water. The pL values are reported in the legend. Solution was stirred during measurement and data were corrected for iR drop.

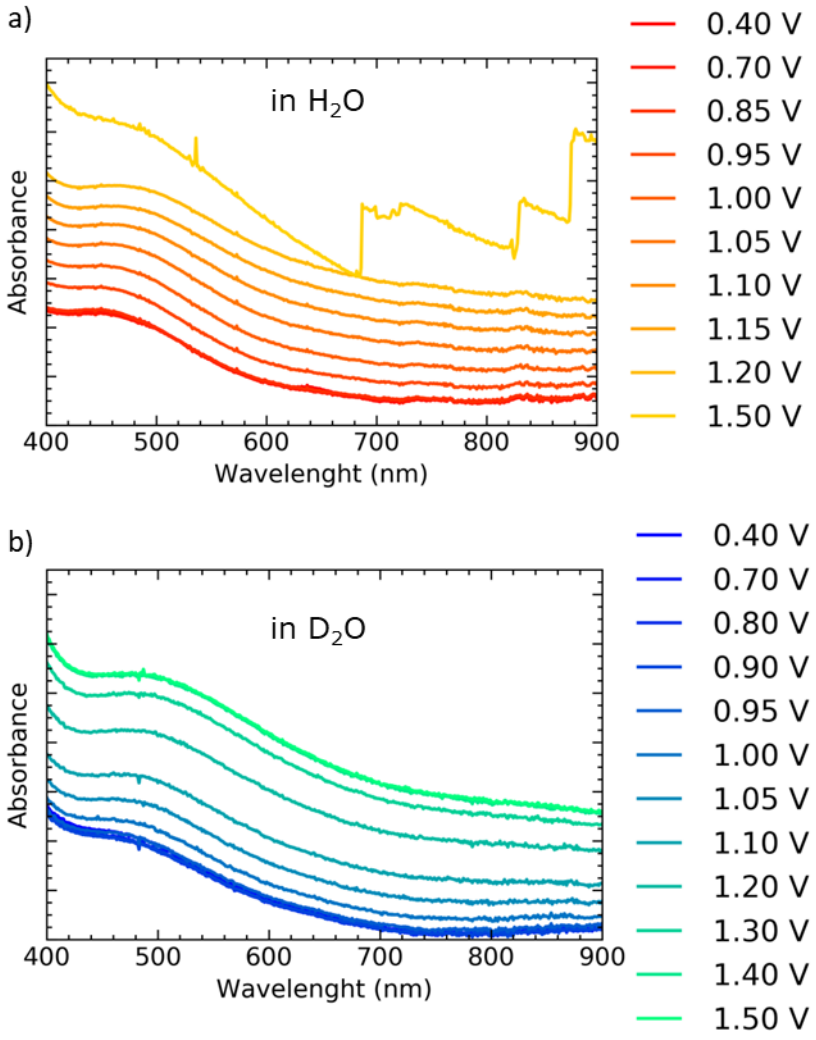

Figure S2. Visible absorption spectroscopy measured in-situ during steady state chronopotentiometry for CoCat in 0.1 M KPi at pL 7 in (a) H_2O-containing buffer and (b) D_2O-containing buffer at different applied potentials (reported in NHE scale after correction for iR drop). Background of blank ITO was subtracted from the data. We observe a wide absorption band between 400 and 700 nm, which increases with increasing potentials. The values for absorbance extracted at 600 nm are shown in Fig. 3b (main text). At the highest potential examined in H_2O-containing buffer bubbles accumulating in the electrolyte contribute to the increase in absorbance. Before extraction of the value at 600 nm the spectrum was corrected from bubbles contribution by subtracting a "bubble factor" to the steady state value. The bubble factor was obtained as the difference in absorption before (electrolyte without bubbles) and after (electrolyte with bubbles) the measurement, obtained at low overpotentials (no direct bubble production).

Table S1. Parameters for the simulation of in-situ visible absorption data measured during step-wise changes between reducing and oxidizing potential.[a, b, c, d]

		In water				In deuterated water			
		Reduction		**Oxidation**		**Reduction**		**Oxidation**	
pL 6	**a1**	0.12	±0.02	0.26	±0.08	0.12	±0.02	0.22	±0.06
	t1	2.29	±0.18	2.57	±0.12	1.92	±0.47	3.05	±0.46
	a2	0.66	±0.11	0.55	±0.06	0.48	±0.18	0.41	±0.13
	t2	0.21	±0.05	0.70	±0.05	0.16	±0.07	0.64	±0.12
	A3	0.0022	±0.0004	-0.0026	±0.0006	0.0020	±0.0007	-0.0028	±0.0005
	B	7.15	±0.14	6.40	±0.25	7.53	±0.50	6.96	±0.63
pL 7	**a1**	0.09	±0.01	0.10	±0.02	0.10	±0.02	0.18	±0.07
	t1	1.67	±0.29	2.18	±0.08	2.04	±0.37	2.25	±0.49
	a2	0.48	±0.10	0.49	±0.07	0.51	±0.17	0.40	±0.13
	t2	0.12	±0.02	0.42	±0.04	0.17	±0.05	0.54	±0.07
	A3	0.0015	±0.0003	-0.0014	±0.0002	0.0016	±0.0004	-0.0019	±0.0006
	B	7.33	±0.05	6.76	±0.09	7.11	±0.14	6.88	±0.67
pL 8	**a1**	0.13	±0.07	0.17	±0.06	0.10	±0.06	0.24	±0.22
	t1	2.06	±0.10	2.17	±0.46	2.38	±0.98	1.99	±0.50
	a2	0.57	±0.14	0.61	±0.21	0.46	±0.20	0.36	±0.18
	t2	0.19	±0.02	0.51	±0.13	0.17	±0.07	0.51	±0.29
	A3	0.0022	±0.0013	-0.0018	±0.0007	0.0021	±0.0016	-0.0019	±0.0010
	B	7.05	±0.47	6.32	±0.67	6.88	±0.79	6.31	±0.90

[a] The "potential jumps" were repeated 30 times and averaged. The time resolution was 10 ms.

[b] Data were simulated as a sum of three exponential plus a constant: $a1 * \exp(-x/t1) + a2 * \exp(-x/t2) + a3 * \exp(-x/t3) + b$.

[c] Due to the slow process represented by the third exponential ($x \ll t3$), we report in the table values for a linear approximation of the third exponential: $a1 * \exp(-x/t1) + a2 * \exp(-x/t2) + A3 * x + B$, obtained from $A3 = -a3/t3$ and $B = b + a3$.

[d] Reported errors are the standard error (95% confidence interval) from three independent measurements.

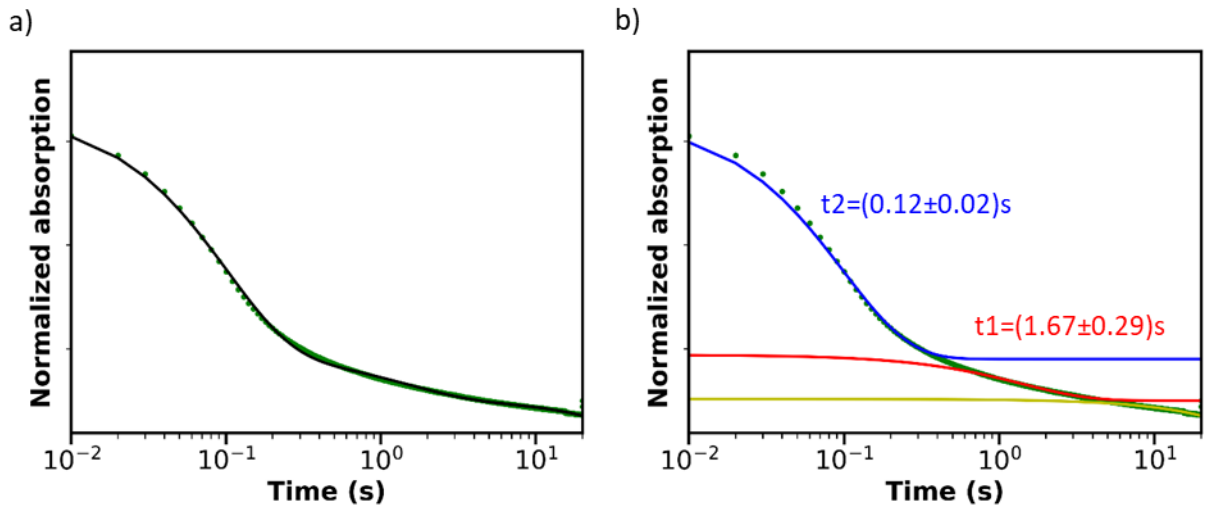

Figure S3. Data for explanatory purposes from time-resolved in-situ visible absorption spectroscopy measured during the reduction step in potential-jumps experiments. The purpose of this figure is to justify the use of three exponential in the simulation of the time behavior. The data shown in a logarithmic scale highlights the three phases that compose the signal and are represented by three exponential function with very different half-times. (a) The simulated curve superimposed on the experimental data. (b) Individual components are plotted together with the experimental curve.

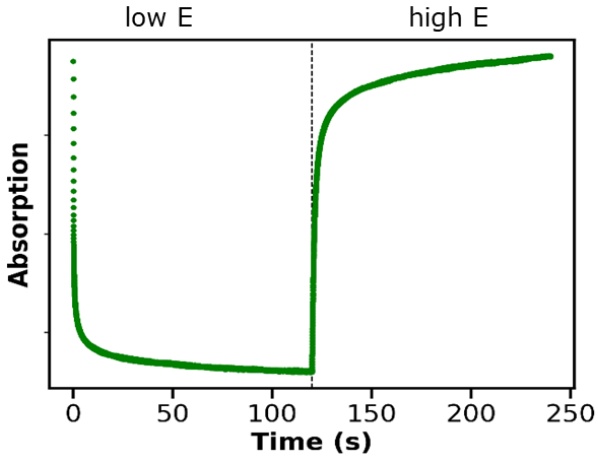

Figure S4. Longer time-resolved in-situ visible absorption data measured during potential jumps between reducing and oxidizing potentials, for CoCat in 0.1 M KPi at pH 7 (H_2O buffer). The signal has not reached a stable level after potential application for 2 min.

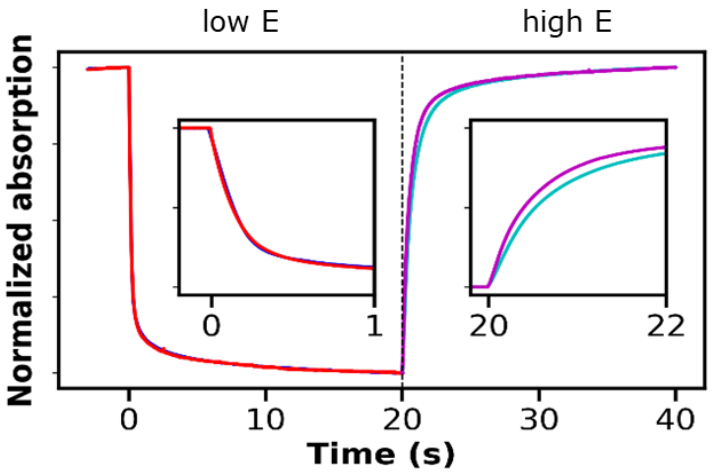

Figure S5. Potential jumps measured with time-resolved in-situ UV-vis spectroscopy between a reducing potential (1.06 V_{RHE}) and an oxidizing potential (1.71 V_{RHE}), for CoCat in 0.1 M KPi H_2O-containing buffer (red and violet lines) or D_2O-containing buffer (blue and cyan lines) at pL 7. The potential applied was the same in water and deuterated water, but no isotopic effect is visible.

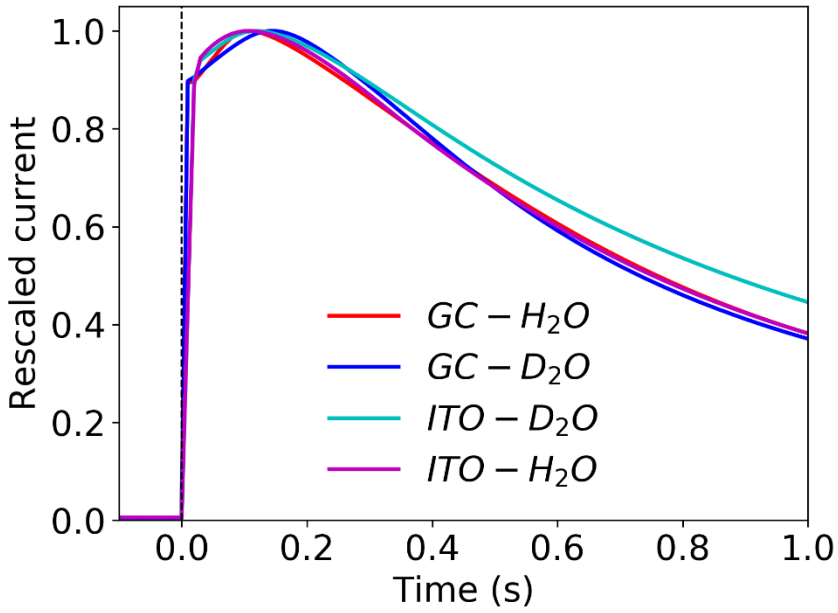

Figure S6. Time-resolved current signal measured during potential jumps between reducing and oxidizing potential, for CoCat in 0.1 M KPi H_2O-containing buffer (red and violet lines) or D_2O-containing buffer (blue and cyan lines) at pL 7. Data were collected on two different substrates: glassy carbon (GC) that has a lower resistance and ITO that has higher resistance. ITO is transparent and therefore is necessary for in-situ collection of visible absorption signal. The higher resistance influences the current at times lower than 20 ms, therefore not affecting the detected half-lifes (lower one at 118 ms). The current was rescaled to achieve a better comparison of the different time courses.

Table S2. Parameters for simulation of Co oxidation state at different applied potential with a modified Nernst equation (Eq. 2, main text). [a, b, c]

	XAS			UV/vis	
	H2O V_{NHE}	D2O V_{NHE}		H2O V_{NHE}	D2O V_{NHE}
E_{m1}	1.01±0.02	1.07±0.02	E_{m1}	1.020±0.002	1.078±0.002
E_{m2}	1.17±0.04	1.22±0.05	E_{m2}	1.189±0.004	1.250±0.003
E_I	47±10 mV		E_I	24±2 mV	
Y_{min1}	2.56		Y_{min1}	2.63	
Y_{max2}	3.25		Y_{max2}	3.26	

[a] Quasi-in-situ X-ray absorption measurements and in-situ visible absorption measurements were used for simulation (data are shown in Fig. 3b in the main text).

[b] In the simulation $E_{m1,2}$ were free to vary, E_I was constrained to have the same value for each data type, $Y_{min1,max2}$ were fixed at the saturation value for each measurement type and $Y_{max1,min2}$ were fixed to 3.

[c] Errors represent one standard deviation obtained with the Bootstrap method.

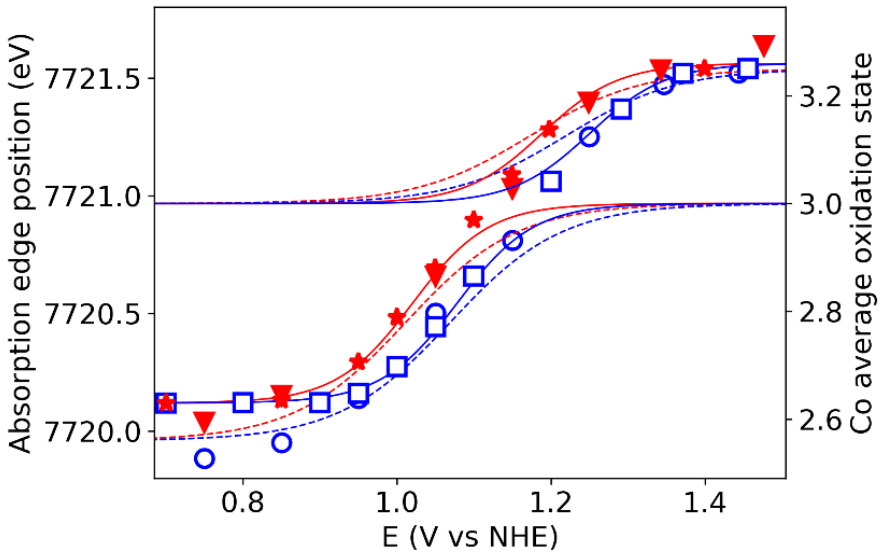

Figure S7. Highlight of the two components derived from Eq. 2 (main text), corresponding to the $Co^{II} \rightleftharpoons Co^{III}$ and the $Co^{III} \rightleftharpoons Co^{IV}$ transitions. The exact equation used for simulation was:

$$Y = \frac{Y_{max,1}e^{f(E,1)}+Y_{min,1}}{e^{f(E,1)}+1} + \frac{(Y_{max,2}-Y_{max,1})e^{f(E,2)}+(Y_{min,2}-Y_{max,1})}{e^{f(E,2)}+1},$$

with $f(E,j) = \frac{E-E_{mj}}{K_B\mathrm{T}+E_I}$ and $Y_{max,1} = Y_{min,2} = 3$.

Changes in Co oxidation state for different applied potential, obtained from freeze-quench X-ray absorption measurements (triangles and circles) and in-situ visible absorption measurements (stars and squares), on CoCat samples in 0.1 M KPi buffer at pL 7 containing H_2O (red) or D_2O (blue). The data were simulated with a sigmoidal curve (solid line for visible and dotted line for X-ray absorption), parameters and results from the simulation are reported in Table 1 and Table S2. The sigmoidal curves representing the sum of the two components are shown in Fig. 3b (main text).

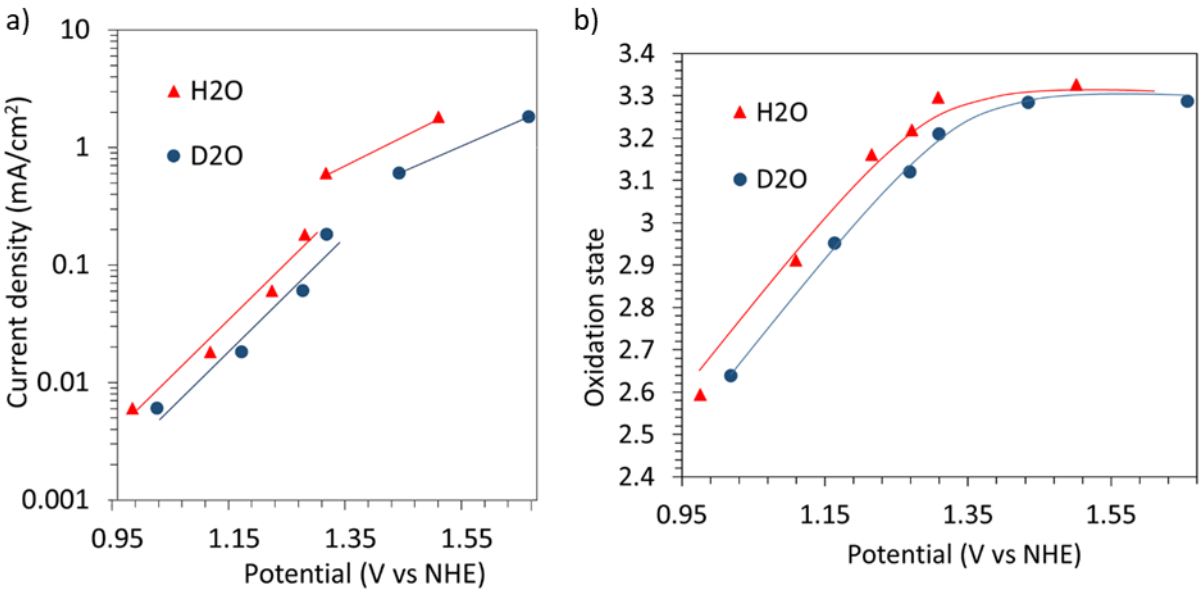

Figure S8. (a) Current density and (b) Co average oxidation state as a function of the applied potential for CoCat in 0.1 M KPi at pL 7 prepared with H_2O (red triangles) or with D_2O (blue circles). Lines were added to guide the eye. Samples were prepared with the freeze-quench method, a fixed current was applied before freezing. The reported potential was measured 1 min before freezing.

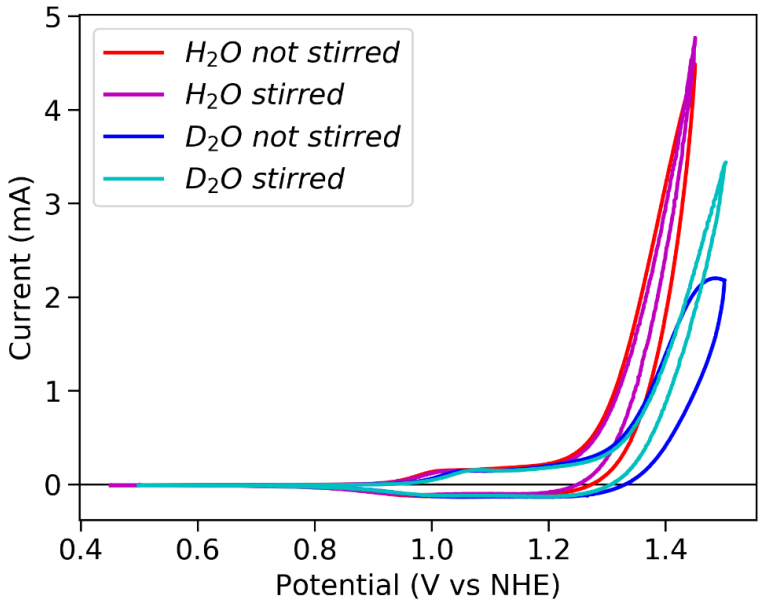

Figure S9. Cyclic voltammetry (20 mVs^{-1}) for CoCat in 0.1 M KPi at pL 7 prepared with H_2O (red and violet lines) or with D_2O (blue and cyan lines), for stirred and not stirred solutions. The effect of stirring is visible at high voltages where mass transport limitations start to influence the catalytic rate. The CV's potential-range was shifted anodically by 50 mV in D_2O, in order to perform the measurements in the same current range.

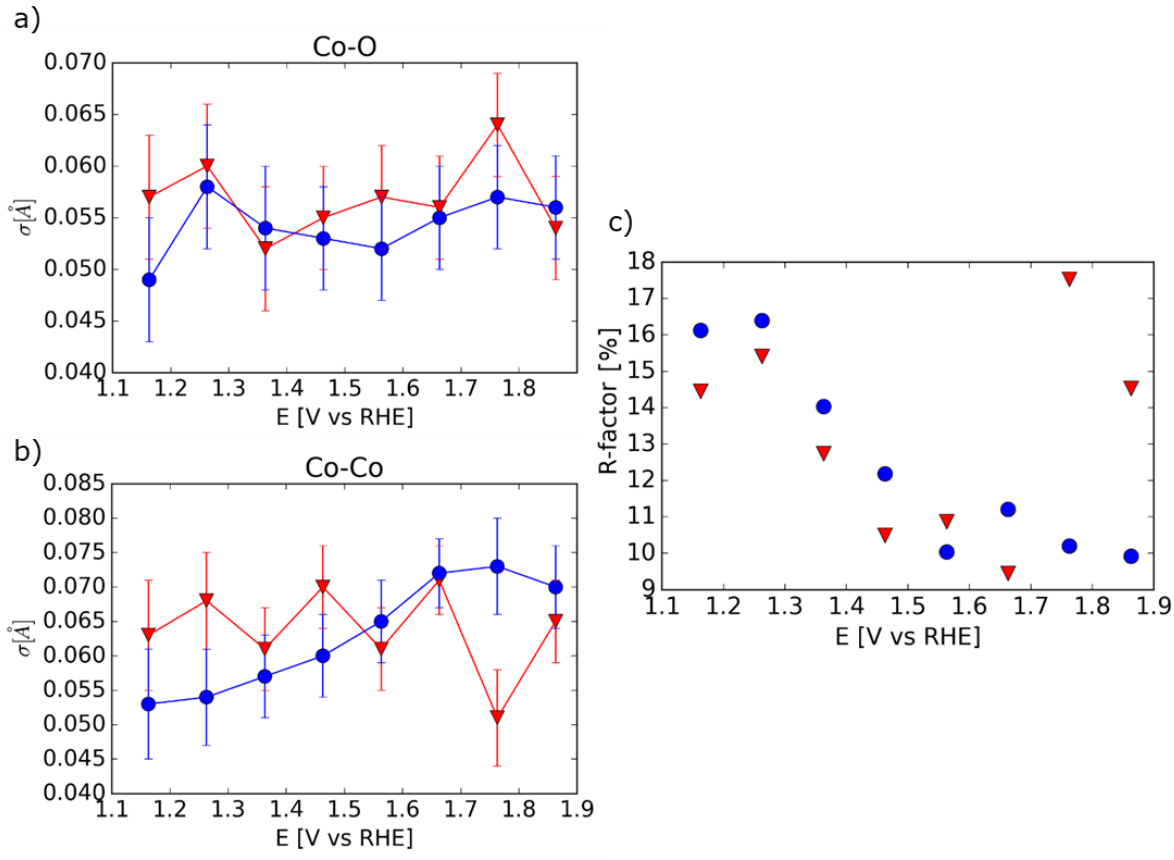

Figure S10. Debye-Waller parameter for (a) Co-O and (b) Co-Co shells simulated on the k^3-weighted EXAFS. (c) R-factor for the reported simulations. Data from X-ray absorption measurements at the Co K-edge for CoCat samples frozen during the application of an oxidizing potential (freeze-quench method) in 0.1 M KPi H_2O buffer (red triangles) or D_2O buffer (blue circles) at pL 7. The other simulation parameters are reported in Fig. 4 (main text). The R-factor is obtained from the sum of the residuals.

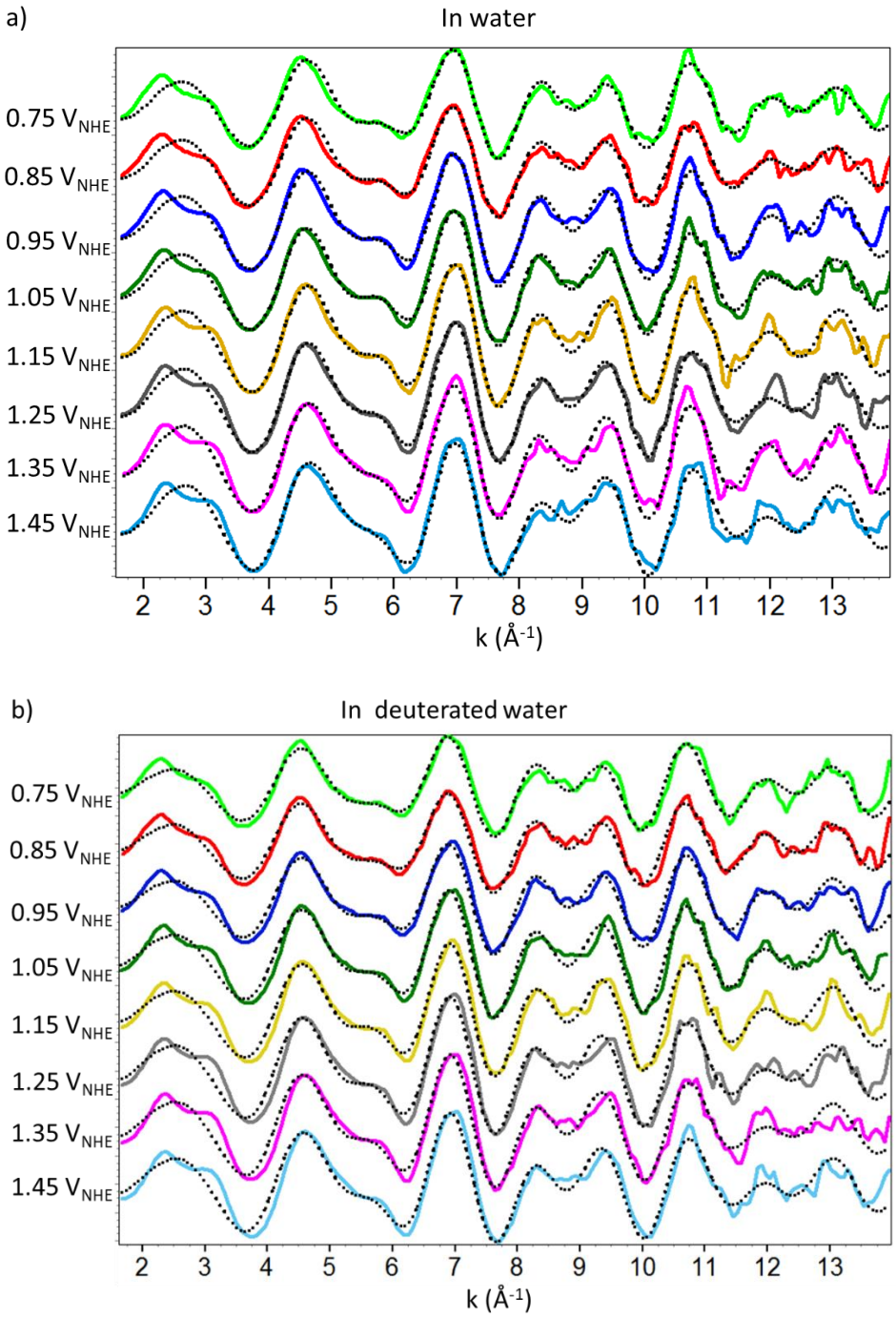

Figure S11. k^3-weighted EXAFS (solid line) and their simulation (dotted line) at the Co K-edge for CoCat in 0.1 M KPi at pL 7 made with (a) H_2O or (b) D_2O. Samples were prepared with the freeze-quench method, the potential applied before freezing are reported on the vertical axis. Simulation results are shown in Fig. S10, Fig. 4 (main text) and listed in Table S3.

Table S3. EXAFS fit results at the Co K-edge for CoCat frozen in-situ in 0.1 M KPi at pL 7 made with H_2O (upper table) or D_2O (lower table). [a, b]

Conditioning potential (V_{NHE}) in H_2O	C-O			Co-Co			R_f (%)
	N	R (Å)	σ (Å)	N	R (Å)	σ (Å)	
0.75	4.9 ±0.3	1.903 ±0.003	0.057 ±0.006	3.2 ±0.5	2.814 ±0.003	0.063 ±0.008	14.4
0.85	5.1 ±0.4	1.901 ±0.003	0.060 ±0.006	3.5 ±0.5	2.817 ±0.003	0.068 ±0.007	15.4
0.95	5.4 ±0.3	1.894 ±0.003	0.052 ±0.006	4.0 ±0.5	2.813 ±0.003	0.061 ±0.006	12.7
1.05	5.6 ±0.3	1.896 ±0.003	0.055 ±0.005	4.6 ±0.5	2.814 ±0.003	0.070 ±0.006	10.5
1.15	6.0 ±0.3	1.887 ±0.003	0.057 ±0.005	4.4 ±0.5	2.812 ±0.002	0.061 ±0.006	10.9
1.25	6.1 ±0.3	1.884 ±0.002	0.056 ±0.005	4.9 ±0.5	2.813 ±0.003	0.071 ±0.005	9.4
1.35	6.4 ±0.4	1.886 ±0.003	0.064 ±0.005	3.6 ±0.4	2.817 ±0.002	0.051 ±0.007	17.5
1.45	6.1 ±0.3	1.877 ±0.002	0.054 ±0.005	3.9 ±0.5	2.813 ±0.003	0.065 ±0.006	14.5
Conditioning potential (V_{NHE}) in D_2O	**C-O**			**Co-Co**			**R_f (%)**
	N	**R (Å)**	**σ (Å)**	**N**	**R (Å)**	**σ (Å)**	
0.75	4.5 ±0.3	1.904 ±0.003	0.049 ±0.007	2.7 ±0.4	2.815 ±0.003	0.053 ±0.009	16.1
0.85	4.8 ±0.4	1.904 ±0.003	0.058 ±0.006	2.7 ±0.4	2.817 ±0.003	0.054 ±0.009	16.4
0.95	5.0 ±0.3	1.900 ±0.003	0.054 ±0.006	3.3 ±0.4	2.814 ±0.003	0.057 ±0.007	14.00
1.05	5.5 ±0.3	1.893 ±0.003	0.053 ±0.006	4.0 ±0.5	2.813 ±0.002	0.060 ±0.006	12.2
1.15	5.6 ±0.3	1.889 ±0.003	0.052 ±0.005	4.5 ±0.5	2.811 ±0.002	0.065 ±0.005	10.00
1.25	6.1 ±0.3	1.886 ±0.002	0.055 ±0.005	5.1 ±0.5	2.812 ±0.003	0.072 ±0.005	11.2
1.35	6.2 ±0.3	1.882 ±0.002	0.057 ±0.005	5 .0 ±0.6	2.809 ±0.003	0.073 ±0.005	10.2
1.45	6.1 ±0.3	1.881 ±0.002	0.056 ±0.005	4.6 ±0.5	2.811 ±0.003	0.070 ±0.006	9.9

[a] Two coordination shells were used with three free parameters each: coordination number (N), distance (R) and Debye-Waller parameter (σ).
[b] The amplitude reduction factor (S_0^2) was 0.7.

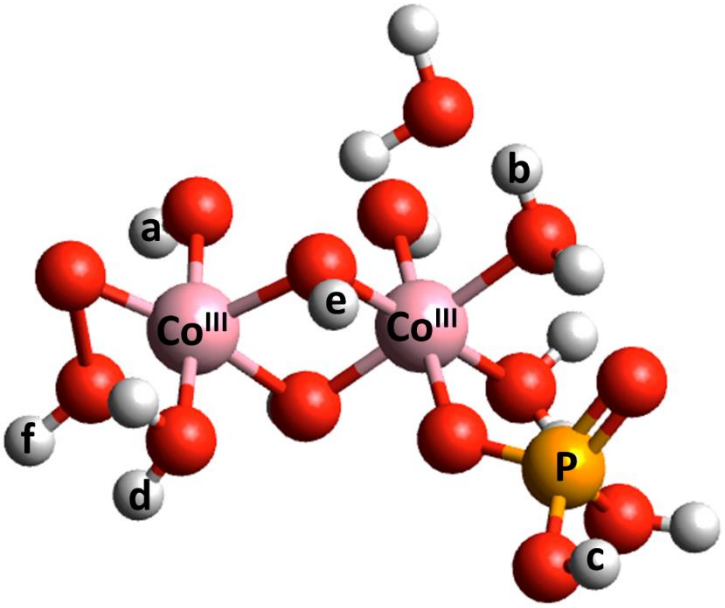

Figure S12. Example of a structure used for DFT calculations. Letters refer to the features explained in Table S4. The mixed structure is only for exemplification purposes: features f, c and b where each part of separately optimized structures.

Table S4. Values for EIE obtained from DFT calculations for differently coordinated protons (details in Method Section and Fig. S12).

Species	Fig. S12	ΔE_{fin}-ΔE_{in} (mV)	ΔpK_a
Co^{II}-OH		26.5	0.45
Co^{III}-OH		29.7	0.50
Co^{III}-Co^{III}-OH	(a)	30.3	0.51
Co^{II}-OH_2		31.6	0.53
Co^{III}-OH		32.6	0.55
Co^{III}-Co^{III}···P-OH	(c)	32.8	0.56
Co^{III}-OH_2		33.5	0.57
Co^{III}-Co^{III}-OH_2	(d)	33.7	0.57
Co^{III}-Co^{III}-OH_2	(d)	33.8	0.57
Co^{III}-OH_2		33.8	0.57
Co^{III}–OH_2···OH_2	(b)	34.3	0.58
Co^{III}-OH···OH_2		34.8	0.59
Co^{III}-OH-Co^{III}	(e)	35.4	0.60
Co^{III}-OH-Co^{III}	(e)	36.6	0.62
Co^{III}-OOH	(f)	40.4	0.68

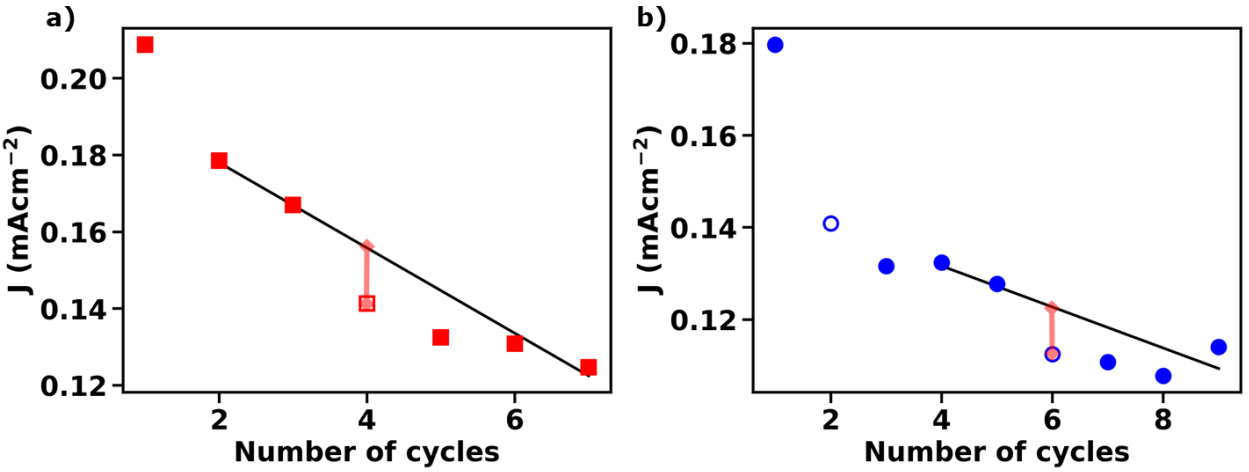

Figure S13. Alternative ways to calculated the $^{16}O/^{18}O$ KIE. Each point represents a potential step (3 min each) in 0.1 M KPi at pH 7 made of either $H_2{}^{16}O$ (closed symbols) or $H_2{}^{18}O$ (open symbols). The solution was exchanged after each protocol repetition consisting in 3 potential steps (1.25, 1.30 and 1.35 V_{NHE}, corrected for resistance drop, 9 min in total). Data are presented only for 1.25 V_{NHE}, because at higher potential mass-transport limitations influence the behavior. (a) and (b) represent two independent repetitions, black lines are a linear regression of points acquired in $H_2{}^{16}O$ (excluded the one directly after $H_2{}^{18}O$ exposure) and represent normal catalyst degradation linked to solution exchange between each point. Red lines connect the point in $H_2{}^{18}O$ with the value it would have had in $H_2{}^{16}O$ and were used to estimate the KIE, we obtained a KIE = 1.10, 1.09 for (a) and (b) respectively. Another value for KIE estimation was obtained from the ratio between the first two points in (b): decrease caused by both KIE and catalyst corrosion, after correction by the percent decrease between the first two points in (a): decrease caused only by catalyst corrosion, we obtained a KIE = 1.10. All alternative methods furnished KIE values compatible with the KIE = 1.11±0.03 found with the method reported in the main text (Fig. 7 and S14).

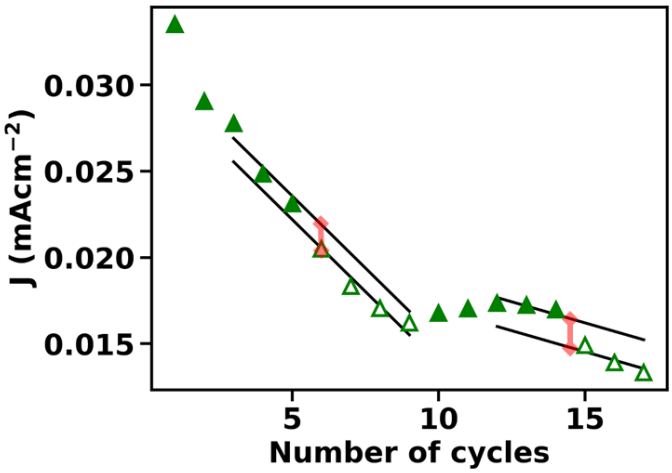

Figure S14. Calculation of the $^{16}O/^{18}O$ KIE at 1.20 V_{NHE}. Each point represents a potential step (3 min each) in 0.1 M KPi at pH 7 made of either $H_2{}^{16}O$ (closed triangles) or $H_2{}^{18}O$ (open triangles). The solution was exchanged after each protocol repetition consisting in 2 potential steps (1.20 and 1.25 V_{NHE}, corrected for iR drop, 6 min in total). Black lines represent the activity decrease due to catalyst degradation and are forced to be parallel between $H_2{}^{16}O$ and $H_2{}^{18}O$ solutions. Red lines indicate the points used to estimate the KIE.

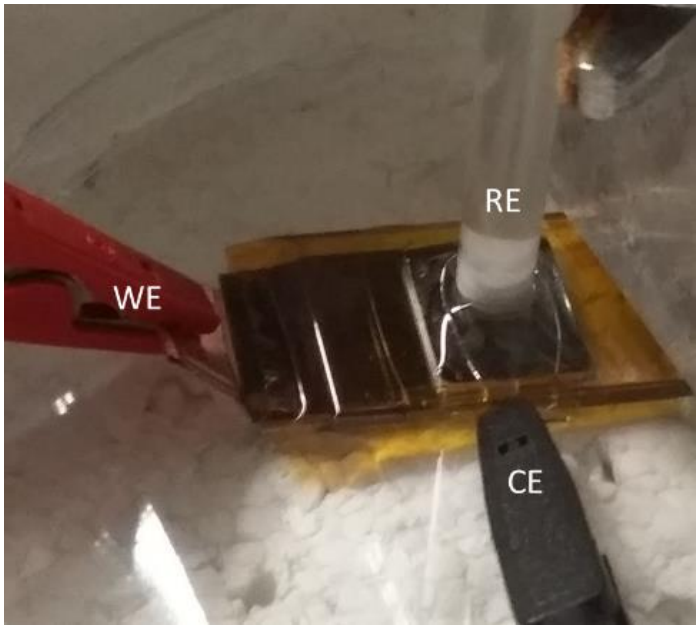

Figure S15. Single-time use electrochemical cell for freeze-quench sample preparation, prior to X-ray absorption measurements. The counter electrode is a Pt wire positioned at a distance of 1 mm from the working electrode (X-ray transparent GC). The reference electrode is a Hg/Hg_2SO_4 (saturated), that is removed before freezing the sample. Further details are given in the method section.